Optical Characterizations and Modelling of Semitransparent Perovskite Solar Cells for Tandem Applications

Conference Paper · October 2019

DOI: 10.4229/EUPVSEC20192019-3BV.2.53

CITATIONS
12

READS
1,230

8 authors, including:

Emilie Raoult
Électricité de France (EDF)
4 PUBLICATIONS **16** CITATIONS
SEE PROFILE

Sebastien Jutteau
Électricité de France (EDF)
22 PUBLICATIONS **72** CITATIONS
SEE PROFILE

Armelle Yaiche
Électricité de France (EDF)
12 PUBLICATIONS **38** CITATIONS
SEE PROFILE

Damien Coutancier
French National Centre for Scientific Research
7 PUBLICATIONS **28** CITATIONS
SEE PROFILE

OPTICAL CHARACTERIZATIONS AND MODELLING OF SEMITRANSPARENT PEROVSKITE SOLAR CELLS FOR TANDEM APPLICATIONS

E. Raoult[1,2,3], R. Bodeux[1,2], S. Jutteau[1,2], S. Rives[1,2], A. Yaiche[1,2], D. Coutancier[2,4], J. Rousset[1,2], S. Collin[2,3]
[1] EDF R&D, 18, Boulevard Thomas Gobert, 91120, Palaiseau, France
[2] Institut Photovoltaïque d'Ile de France (IPVF), UMR 9006,18 Boulevard Thomas Gober128, 91120 Palaiseau, France
[3] Centre for Nanoscience and Nanotechnology (C2N), CNRS, Université Paris-Saclay, 91120 Palaiseau, France
[4] CNRS, UMR 9006, 18, Boulevard Thomas Gobert, 91120 Palaiseau, France

ABSTRACT: Optical properties of perovskite based tandem solar cells are reported. The 4-terminal tandem has been built with 21.7 % of efficiency, combining semitransparent perovskite solar cell (PSC) with a commercially-available Aluminum Back Surface Field (Al-BSF) silicon solar cell. That silicon solar cell presents PCE of 18.5% to generate an overall 4 T tandem efficiency of 21.7 % in combination with a semitransparent perovskite solar cell (PSC) of 16.6%. Optical losses have to be minimized through the PSC in the near infrared region to optimize the efficiency of the silicon cell. However, optical properties of layers composing the PSC are poorly identified, and they roughly depend on the composition of materials and their fabrication. That is why this work aims to perfectly characterize each layer of the semitransparent PSC by spectrophotometry, profilometry and ellipsometry measurements, in order to determine their optical indices n and k. Particularly, we report for the first time the optical indices of the $Cs_{0.05}(MA_{0.166}FA_{0.833})_{0.95}Pb(Br_{0.166}I_{0.833})_3$ triple cation perovskite. Optical modelling based on the transfer matrix method is used for the identification of the optical losses. These results will allow to precisely design the devices and to quickly test the interest of various materials, by predict their impact on the efficiency of the bottom silicon cell and the tandem cell.
Keywords: Perovskite, Tandem, Optical Properties, Modelling

1 INTRODUCTION

Recently hybrid organic-inorganic perovskites are regarded as promising absorber materials for future PV systems on a terawatt scale. The latest power conversion efficiency (PCE) record of 24.2% has encouraged numerous investigations to develop low-cost manufacturing processes [1]. Furthermore, these materials show a wide band gap greater than 1.5 eV that is interesting for top cell absorbers in tandem applications. Recently, PCE of 28% has been achieved by the combination of a perovskite top cell and a crystalline silicon bottom cell [2].

4-terminal tandem has been built in our lab combining semitransparent $Cs_{0.05}(MA_{0.166}FA_{0.833})_{0.95}Pb(Br_{0.166}I_{0.833})_3$ triple cations perovskite solar cell (PSC) with a commercially-available Aluminum Back Surface Field (Al-BSF) silicon solar cell [3]. The efficiency reaches 22.3% but it is always lower than the Shockley-Queisser limit for one junction cell. To further improve the efficiency, parasitic optical losses have to be minimized, mainly in the near infrared region (NIR) in order to keep a high efficiency for the silicon bottom cell. Optical characterizations and modelling help to understand where happen the losses inside the cell and are already done by different groups [4 -11]. The most time, optical modelling is based on path light simulation with the Matrix Transfer Method which works with the optical indices n and k, and the thickness of each layer of the stack [12-13]. It could be also used to design precisely the thickness or roughness of each layer [7], test different materials [10], show the effect of the modification the perovskite band-gap [4,9,11] or even coupled with electrical model.

However, Jiang shows that the optical indices of the materials which composed the PSC can change with the composition and the fabrication, especially the perovskite layer [10]. Thus, to have a very good fitting of the experimental data, it is not possible to take the indices in literature. In fact, to the best of our knowledge, no work on triple cations perovskite can be found.

For these reasons, we report here the optical modeling of the semitransparent PSC, after the characterization of the optical indices of each layer, including those of the triple cation perovskite. After a long iterating process to find the suitable optical indices for each layer. The path light is exactly modelled inside the cell.

2 METHOD

2.1 Semitransparent PSC fabrication

A compact/mesoporous TiO_2 bilayer has been deposited at 450 °C using a precursor solution made of titanium diisopropoxide on commercial substrate from Solems, composed by Fluor doped SnO_2 (FTO)-coated on a soda lime glass 3mm called TEC7. On similar substrates, different groups report the presence of SiO_2 and SnO_2 between glass and FTO layers. [5, 10]

$Cs_{0.05}(MA_{0.166}FA_{0.833})_{0.95}Pb(Br_{0.166}I_{0.833})_3$ perovskite solution was deposited by spin coating and annealed at 100 °C. A solution of Spiro-OMeTAD has been deposited by spin coating. In the case of opaque cells, 100 nm of Au were thermally evaporated under high vacuum. For semitransparent devices, 90% In_2O_3 - 10% SnO_2 (ITO) has been deposited by RF magnetron sputtering. Over ITO cathodes, a U-shape pattern of Au (~100 nm thick) was thermally evaporated over the edges of ITO area in order to minimize the series resistance.

Following the same process, monolayer samples were synthesized: a single layer (TiO_2, perovskite, Spiro or ITO) is deposited on soda lime glass for characterizations. For the subtract TEC7, the top layer of FTO is remove with DMF solution.

2.2 Characterization

PSC are measured in superstrate condition for all the characterizations.

J-V curves under illumination have been registered using a digital source meter (Keithley Model 2400) and an AAA sun simulator (Oriel Sol3A) as light source (AM1.5 G spectra and 1 Sun intensity).

External quantum efficiency (EQE) has been measured using an Oriel IQE200 system connected with a source meter (Keithley 2400).

An Uvisel 2 from Horiba ellipsometer was used to measure the optical parameters of the different layers of PSC.

A spectrophotometer (Agilent Cary 5000) has been used to measure the transmission T and the reflection R between 200 and 1300nm of the different samples. The absorption A is obtained by the following equation: $A(\lambda) = 100 - R(\lambda) - T(\lambda)$.

Cross section picture and thickness has been with a Scanning Electron Microcopy (ZEISS), after splitting the PSC and the metallization of the section with Carbone deposition.

Thickness has been also obtained on a profilometer (Dektak).

2.3 Simulation and iterative scheme

An iterating process has been used to find correct optical indices (the refractive index n(λ) and the extinction coefficient k(λ)) for each layer. It can be seen in Fig. 1.

First, the thickness of each monolayer sample is precisely characterized by profilometer. Combined with an ellipsometry measurement, a model of the optical indices of the materials is created with the software DeltaPsi, developed by Horiba Jobin Yvon. This dispersion models are based on different mathematical formulas like the Cauchy dispersion law [14], the Tauc-Lorentz dispersion formulae [15] or the New Amorphous dispersion formulae which was derived by Horiba Jobin Yvon on the basis of Forouhi-Bloomer formulation [16]. The choice of the dispersion model depend on the type of material (amorphous, polymers, semi-conductors, dielectrics, metals, insulators, …) and how it is supposed to absorb the light (intra-band absorption, quantum effect, …) as shown in Table I.

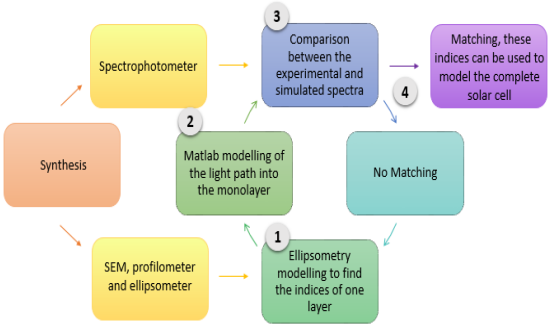

Figure 1: Methodology process to find the correct optical indices with the iteration cycle.

Table I: Dispersion models for ellipsometry modeling

	Models of dispersion [17]
Glass (TEC7)	Cauchy
SnO_2 (TEC7)	Classical
SiO_2 (TEC7)	Classical
FTO (TEC7)	New Amorphous + Drude
TiO2	Cauchy
Perovskite	5x Tauc Lorentz
Spiro	4x Tauc lorentz + Oscillator
ITO	2*New amorphous + Drude model

Then, optical properties of PSC, such as transmission, reflection and absorption, have been modelled using a Matlab code developed by the McGehee group at Standford [18] and based on the transfer matrix method which uses the optical indices of the materials to derive the modulus of the electric fields. The program derive the modulus of the electric field in each point of the cell for each wavelength, and gives the transmission, the absorption and the reflection of the stack.

The comparison of the modelled results with the ones obtained on the spectrophotometer validates or not the optical model. We consider a limit at 5% for the Mean Absolute Error (MAE) of the simulated data in comparison with the experimental data, obtained by the following equations:

$$MAE_{Transmission}(\%) = \frac{\sum_{i=300}^{1200} |T_{simu}(i) - T_{exp}(i)|}{901}$$

$$MAE_{Reflection}(\%) = \frac{\sum_{i=300}^{1200} |R_{simu}(i) - R_{exp}(i)|}{901}$$

$$MAE_{Absoprtion}(\%) = \frac{\sum_{i=300}^{1200} |A_{simu}(i) - A_{exp}(i)|}{901}$$

If the MAE is superior at 5%, it is necessary to modify the optical model and try again. If it is correct, the optical indices found can be used for the model of the complete PSC.

3 SYNTHESIS AND CHARACTERIZATION

3.1 Tandem solar cell

J-V curves are shown in Fig. 2.A for semitransparent PSC and silicon devices. PSC and silicon devices exhibit 16.6 % and 18.5% respectively, without hysteresis.

External quantum efficiency (EQE) measurements are shown in Fig. 2.B for semitransparent PSC and filtered silicon devices (PSC are used as top filters for bottom silicon cell). The EQE spectra exhibit a maximum of 80 % and 70 % for the semitransparent PSC and filtered Si cell, respectively. This indicates that optical losses reduce the absorption of the perovskite layer below the band gap at 750 nm and the transmission through the PSC above 750 nm. In addition, an interference pattern is clearly visible on the silicon EQE, and decrease its efficiency.

The theoretical efficiency η_2 of the filtered silicon cell is obtained with its EQE spectrum and the IV measurement of the unfiltered cell. Assuming the FF unchanged, the PCE can be derived from the following equations [19]:

$$J_{sc2} = -q \int_{\lambda_2}^{\lambda_1} EQE_2(\lambda)\phi(\lambda)d\lambda$$

$$V_{oc2} = ln\left(\frac{J_{sc2}}{J_{sc1}}\right) * \frac{k_b T}{q} + V_{oc1}$$

$$\eta_2 = \frac{J_{sc2} V_{oc2} FF_1}{P_{in}}$$

Silicon cell shows a final overall PCE of 5.1%. Finally, 4T tandem efficiency of 21.7% is obtained when combining the PSC and the filtered silicon cell. The calculation, assuming light filtered by the band-gap of our perovskite (750nm) and a PSC fully transparent in NIR, gives a silicon cell with a PCE of 9,8%. This is the maximum that could be achieved without optical losses. Thus, it is necessary to reduce this losses to improve the efficiency of the tandem cell.

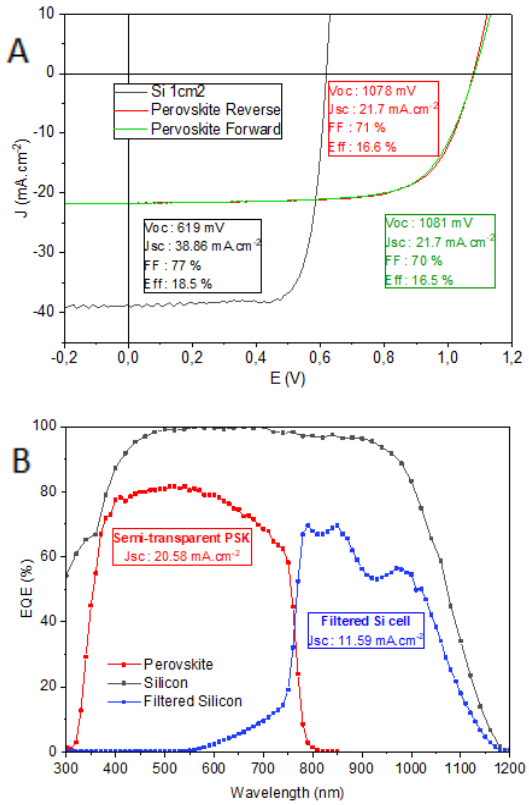

Figure 2:.A IV curves of the semi-transparent PSC, the unfiltered silicon cell. B. EQE of the semi-transparent PSC, the unfiltered and the filtered silicon cell by the PSC.

3.2 Structure of PSC

The stack of the PSC is shown on the SEM cross section in Fig.3.A. The thickness measurements of the different layers have been made for the complete solar cell. However, important variations have been identified on SEM measurements. They are probably due to the cleavage of the glass substrate, necessary to observe the cross section of the cell with the SEM. Thus, the thickness of the layers has been measured by profilometer on monolayers deposited on glass. A comparison with profilometer measurements can be seen on Table II. There is not important roughness at the surface of the cell: the sample is flat. Of course, the interface between mesoporous TiO2 and perovskite needs to be considered a mix of these two layers.

In addition, the substrate TEC7 can be assumed to be a multilayer stack since there are at least three different layers on the SEM image, according to the literature [5, 10].

3.3 Optical properties of PSC

Absorption, transmission and reflection spectra of PSC are shown in Fig. 3.B. Due to the absorption of the perovskite layer, transmission start only at 500 nm. It increases slowly until the perovskite band gap of 750 nm. This sub-gap transmission is caused by a too thin perovskite layer. Above the band-gap, transmission reach quickly 72% at 820nm and slowly decrease in the NIR. The interference pattern is visible and also appears in the filtered silicon EQE (Fig. 2.B).

The reflection spectra is constant at 6.5% between 400 and 750 nm, which corresponds at the perovskite absorption range. Interference patterns are visible in the NIR but also between 300 and 400 nm.

Finally, absorption in NIR region is important with 30% at 1000 nm. It reaches 93% between 300 and 500 nm, and cause no transmission in this region.

These spectra do not take into account the impact of each layer on absorption and transmission, as well as the multiple reflections into the structure, which can cause additional losses. In order to identify the interfaces which can cause the most damages, modelling is required.

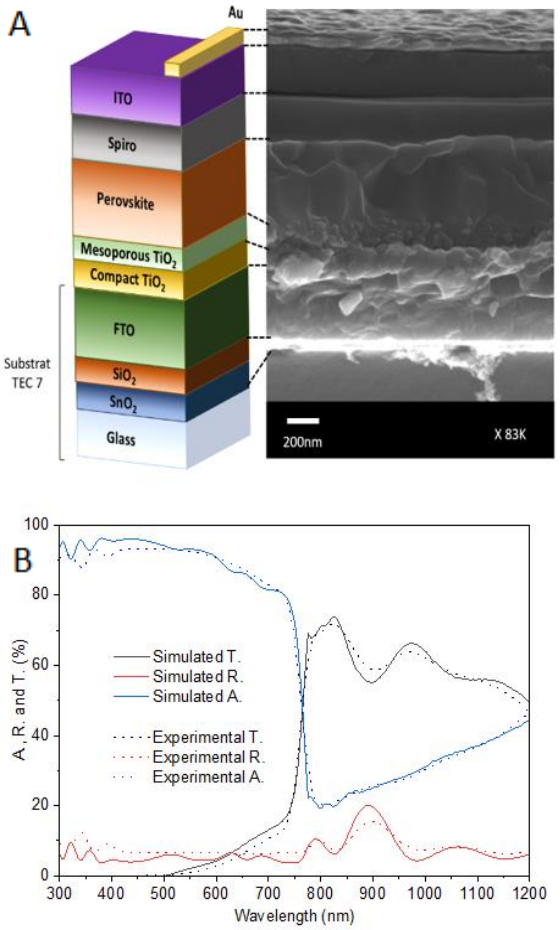

Figure 3:.A Structure of the semi-transparent PSC with a SEM picture of the cross section of the PSC. B. Simulated and experimental data of the transmission, absorption and reflection of the PSC.

Table II: Thickness of the different layers

	SEM for the perovskite solar cell	Profilometer for the monolayer samples
SnO_2	10 nm	-
SiO_2	35-40 nm	-
FTO	462–520 nm	506 nm
Compact TiO2	43-68 nm	-
Mesoporous TiO2	90-110 nm	-
Perovskite	459–644 nm	570 nm
Spiro	208-275 nm	306 nm
ITO	248-281 nm	274 nm

4 SIMULATION ON MONOLAYER DEPOSITED ON GLASS

4.1 Comparison between simulated and experimental data

Simulated and experimental spectra of transmission (T), reflection (R) and absorption (A) for each monolayer are shown in Fig. 4. A very good fit can be observed between the Matlab model and the experimental data for all the monolayer samples with MAE always inferior at 4%, show in Table III.

In fact, all the main optical interference figures fit with the experimental data. In particularly, Fig. 4.A shows the case of the substrate TEC 7. This structure has been modelled with four different layers: a first soda lime glass layer of 3mm, then a SnO_2 layer of 8nm, a SiO_2 layer of 40nm and finally, a FTO layer of 506nm.

For the mesoporous TiO_2 layer, two model are tested. The first one considered the mesoporous TiO_2 as a compact and flat layer, but the second take in account that the layer is porous.

Figure 4: Simulated and experimental spectra of transmission, reflection and absorption for monolayer : TEC7 with FTO (A), TEC7 without FTO (B), compact TiO2 (C), mesoporous TiO2 (D), perovskite (E), spiro (F), sodalime glass (G) and ITO (H)

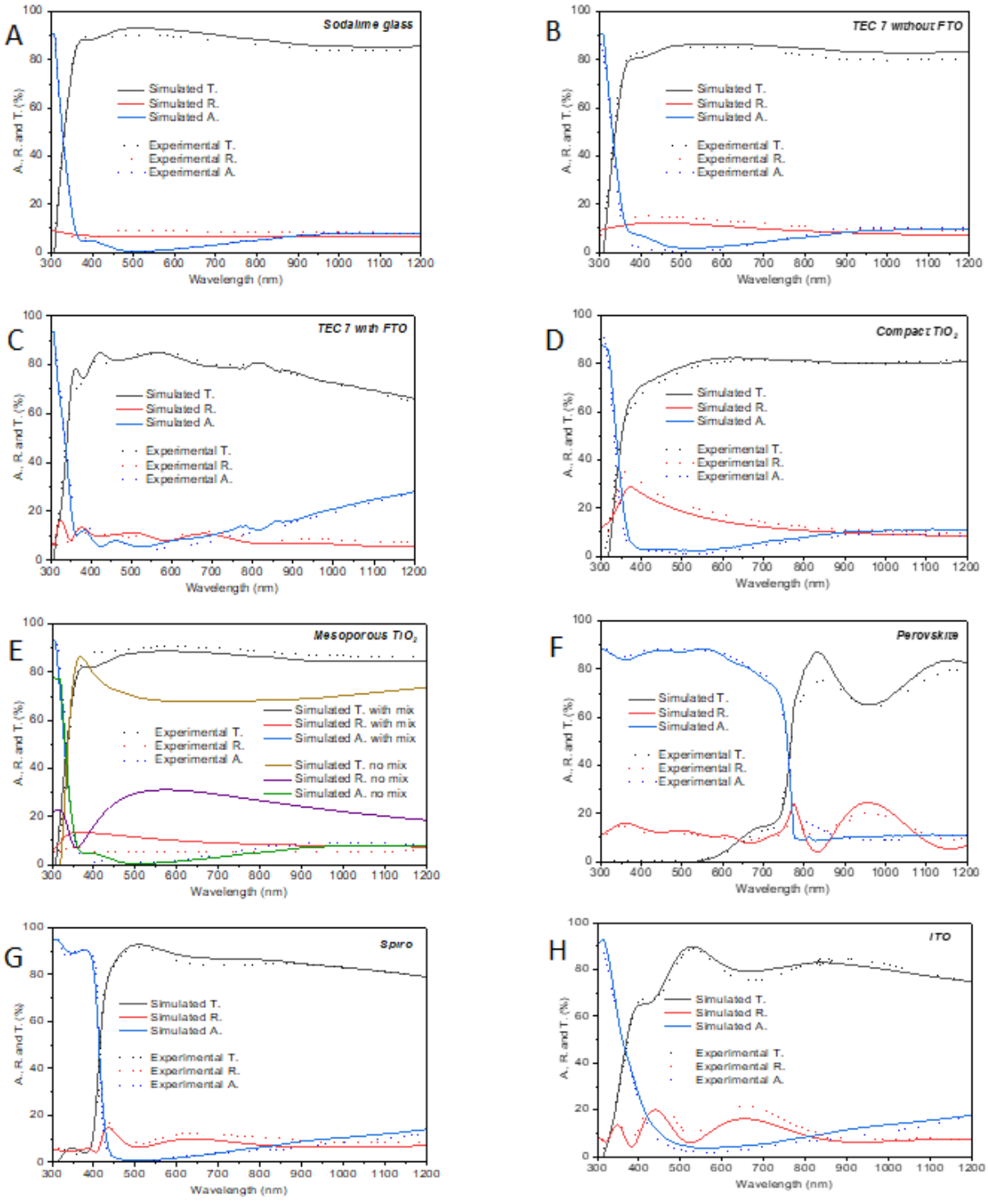

In it, a new layer called "mix layer" is used to take into account the fact that the air and the mesoporous TiO_2 are mixed. The optical indices of the mix layer are a combination of those of air and mesoporous TiO_2. The Fig. 4.E and the Table III clearly show that the second model is required to fit the transmission and reflection spectra because it decrease the intensity of interference figures.

Some monolayers have also great interferences like perovskite or ITO (Fig. 4.F and 4.H). As it is due to the interfaces between this layer with the glass and the air, this interferences can be completely different in a complete PSC. This is why modelled are necessary.

Table III: Mean Absolute Error (MAE) of simulated data in comparison with the experimental data for the transmission (T), reflection (R) and absorption (A), for each monolayer sample and the semi-transparent PSC.

	T (%)	R (%)	A (%)
Glass	1,84	1,86	-
TEC7 without FTO	2,49	2,15	1,67
TEC7 with FTO	1,31	1,69	1,93
Compact TiO2	1,35	2,42	1,89
Mesoporous TiO2 No mix	16,94	18,56	1,46
Mesoporous TiO2 With mix	2,46	3,86	1,39
Spiro	1,43	2,19	1,47
ITO	1,92	2,52	2,21
Semi-transparent PSC	1,40	1,84	1,42

4.2 Optical indices

The final optical indices n and k used for modelling all the layers deposited on glass are presented on the Fig.5.A and B. The values found are consistent with what exists in the literature and with what is known about these materials, even if there are some peculiarities.

For example, FTO is known as a transparent conductive oxide which absorb a lot in IR region, more than ITO. However, his k index is lower than the ITO one in this region. As FTO is the first layer of the stack, it has been fully optimized, contrarily to ITO which has not been annealed here, and does not have its best properties. The differences between the indices of compact and mesoporous TiO_2 can also be explained by the fact that optical indices of the materials can change with the process of fabrication.

Fig. 6.A and B compare the indices n and k of our perovskite confirmed that there are differences for a same formulae like simple cation perovskite MAPbI or double cation CsFaPbIBr. Moreover, refractive index n of CsFaPbIBr seems higher than the CsMAFaPbIBr one by the substitution of FA by MA, whereas the extinction coefficient k is similar at double cation perovskite.

5 MODELIZATION OF THE COMPLETE SOLAR CELL

5.1 Comparison between experimental and simulated data

N et k indices obtained for the monolayer deposited on glass are used in the final model of the PSC.

Fig. 3.B shows the modelling, compared with the experimental data in the superstrate configuration. A very good fit is obtained for absorption, transmission and reflection.

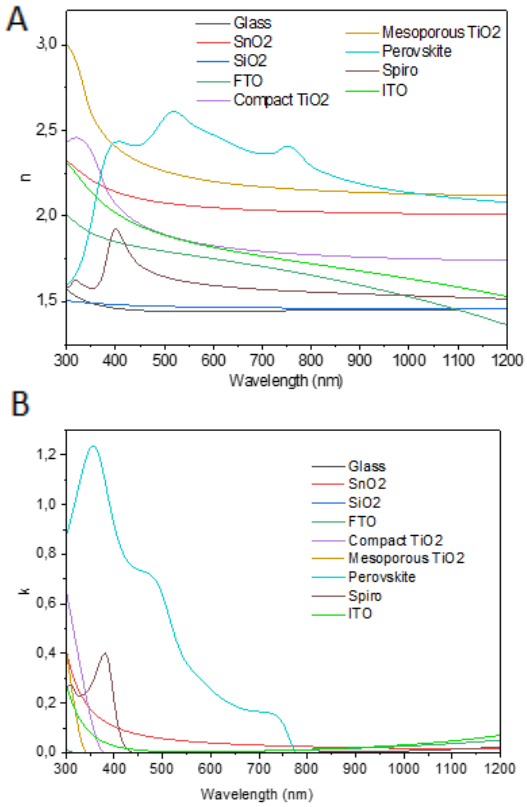

Figure 5: Final optical indices n (A) and k (B) for the different lavers of the PSC

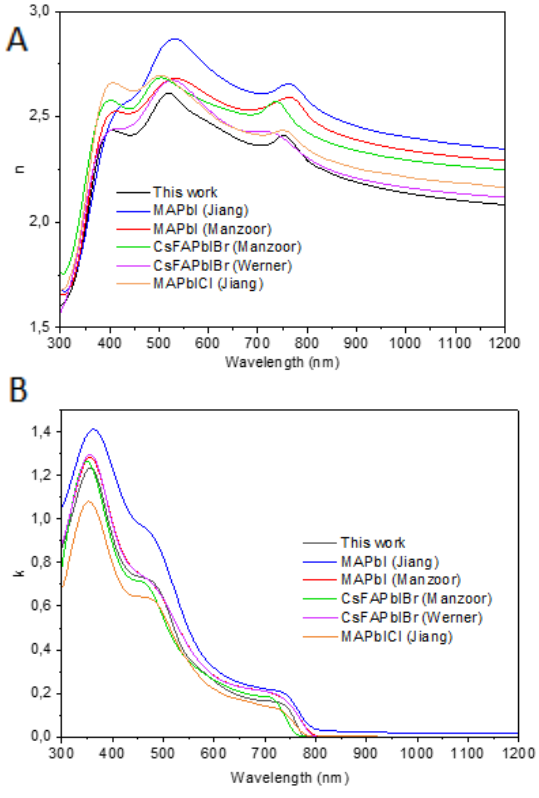

Figure 6: Comparison of the indices n (A) and k (B) for our perovskite CsMAFAPbBrI with other types of perovskite in the literature

The fact that the inference figures are really close to each other is an evidence of the correctness of the indices and the thickness of each layer, even if he refection is slightly lower in our model between 400 and 800nm. This is confirmed by MAE, which are low for the transmission and absorption with respectively 1.40% and 1.42%, and slightly higher for the reflection with 1.84%.

For the mesoporous TiO_2, an additional layer called "mix layer" is used similarly to the monolayer deposited on glass. However, air have been substituted by a perovskite layer in the PSC. Thus, the optical indices of the mix layer are a combination of those of perovskite and mesoporous TiO_2.

5.2 Parasitic absorptions

Fig. 7 shows the distribution of the absorption into the PSC between the different layers.

In the visible region, perovskite absorbs most of the light (A=80%) below the band gap at 750 nm. All others absorptions in this region may be considered parasitic absorptions because they have an impact on the efficiency of the PSC. It is the case with the part of light (A=8% at 550 nm) absorbed by the layers of the substrate TEC7.

In the UV region, the absorption of the perovskite is first limited by the parasitic absorption of TiO_2, which show a smaller band gap than the SnO2 and the glass, at 350 nm.

Finally, in IR region, FTO is clearly the compound which causes the highest parasitic absorption, A=10 % at 1000 nm, while the glass, ITO and spiro, contributes to 8 %, 7% and 2% of absorption, respectively.

However, parasitic absorptions are not the only optical loss factors. Reflection is the second major source of loss after FTO absorption with A=20% at 800 nm, thus identify the interfaces issues is crucial.

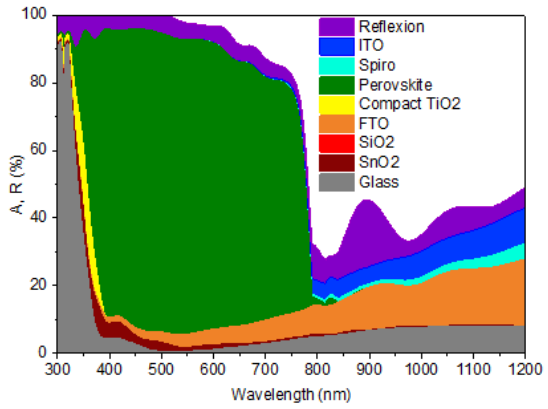

Figure 7: Distribution of the absorption into our PSC between the different layers. In white, the transmission spectrum appears reversed

5.3 Parasitic reflection

Some interfaces are responsible for strong reflections due to poor coupling refractive index between the materials. Fig. 8 shows the reflection at each interface.The reflection at the air/glass interface is responsible for 4% of the total reflection.

The glass-SnO2 and SnO_2-SiO_2 interfaces also seems to be responsible for reflection. However, it is an artefact based on the calculation of the reflection at the interfaces, different from the one included in the transfer matrix for the total reflection. Indeed, the reflection is calculated by considering two infinite layers. On very thin layers of 8 nm like SnO_2, this approximation is no longer possible. Although the Fresnel coefficient for reflected light at the surface is high, the field continuity requirement at the interface is responsible for the development of an evanescent wave within the thin film. Due to the very small thickness of the film, a large part of this evanescent wave reaches its rear face by tunnel effect and spreads into the stack. Thus, the reflection is lower than the calculated one (take into account in the global model).

Finally, the highest parasitic reflection in NIR come from the interface ITO – Air.

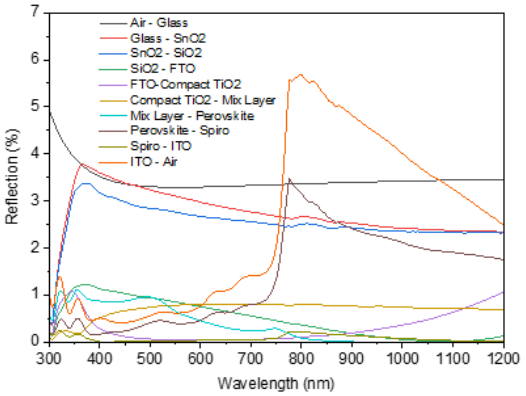

Figure 8: Reflection of each interface of our PSC in function of the part of light which reach it.

6 CONCLUSION

In this study, we have shown how to obtain an accurate optical model of the semi-transparent PSC based on experimental results. It has been possible with a rigorous iteration process of optical indices by combining ellipsometer and spectrophotometer measurements and modeling on Matlab. The optical index for the triple cation mix perovskite has been identified that are not available in the literature.

Optical losses in the PSC has been analyzed. NIR absorption is mainly caused by the electrodes (ITO and FTO), spiro and the glass substrate. Furthermore, the air–glass and ITO-air interfaces are responsible of parasitic reflection.

Acknowledgements *This project is supported at IPVF by the French Government in the frame of Programme d'Investissement d'Avenir – ANR-IEED-002-01.*

REFERENCES

[1] E. H. Jung *et al.*, « Efficient, stable and scalable perovskite solar cells using poly(3-hexylthiophene) », *Nature*, vol. 567, nº 7749, p. 511-515, mars 2019.

[2] « Oxford PV perovskite solar cell achieves 28% efficiency ». .

[3] F. J. Ramos *et al.*, « Highly efficient MoOx-free semitransparent perovskite cell for 4 T tandem application improving the efficiency of

commercially-available Al-BSF silicon », *Sci. Rep.*, vol. 8, nº 1, déc. 2018.
[4] J. Werner *et al.*, « Complex Refractive Indices of Cesium–Formamidinium-Based Mixed-Halide Perovskites with Optical Band Gaps from 1.5 to 1.8 eV », *ACS Energy Lett.*, vol. 3, nº 3, p. 742-747, mars 2018.
[5] J. M. Ball *et al.*, « Optical properties and limiting photocurrent of thin-film perovskite solar cells », *Energy Environ. Sci.*, vol. 8, nº 2, p. 602-609, févr. 2015.
[6] J. Zhao *et al.*, « Is Cu a stable electrode material in hybrid perovskite solar cells for a 30-year lifetime? », *Energy Environ. Sci.*, vol. 9, nº 12, p. 3650-3656, nov. 2016.
[7] M. van Eerden *et al.*, « Optical Analysis of Planar Multicrystalline Perovskite Solar Cells », *Adv. Opt. Mater.*, vol. 5, nº 18, p. 1700151, sept. 2017.
[8] Q. Lin, A. Armin, R. C. R. Nagiri, P. L. Burn, et P. Meredith, « Electro-optics of perovskite solar cells », *Nat. Photonics*, vol. 9, nº 2, p. 106-112, févr. 2015.
[9] S. Manzoor *et al.*, « Optical modeling of wide-bandgap perovskite and perovskite/silicon tandem solar cells using complex refractive indices for arbitrary-bandgap perovskite absorbers », *Opt. Express*, vol. 26, nº 21, p. 27441, oct. 2018.
[10] Y. Jiang *et al.*, « Optical analysis of perovskite/silicon tandem solar cells », *J. Mater. Chem. C*, vol. 4, nº 24, p. 5679-5689, 2016.
[11] Y. Jiang, M. A. Green, R. Sheng, et A. Ho-Baillie, « Room temperature optical properties of organic–inorganic lead halide perovskites », *Sol. Energy Mater. Sol. Cells*, vol. 137, p. 253-257, juin 2015.
[12] L. A. A. Pettersson, L. S. Roman, et O. Inganäs, « Modeling photocurrent action spectra of photovoltaic devices based on organic thin films », *J. Appl. Phys.*, vol. 86, nº 1, p. 487-496, juin 1999.
[13] P. Peumans, A. Yakimov, et S. R. Forrest, « Small molecular weight organic thin-film photodetectors and solar cells », *J. Appl. Phys.*, vol. 93, nº 7, p. 3693-3723, mars 2003.
[14] A.-L. Cauchy, « Sur la réfraction et la réflexion de la lumière », *Bulletin de Férussac*, p. 9, 1830.
[15] G. E. Jellison et F. A. Modine, « Parameterization of the optical functions of amorphous materials in the interband region », *Appl. Phys. Lett.*, vol. 69, nº 3, p. 371-373, juill. 1996.
[16] A. R. Forouhi et I. Bloomer, « Optical dispersion relations for amorphous semiconductors and amorphous dielectrics », *Phys. Rev. B*, vol. 34, nº 10, p. 7018-7026, nov. 1986.
[17] « Horiba Technical Notes about the different models of dispersion on spectroscopic ellipsometry. », .
[18] G. F. Burkhard, E. T. Hoke, et M. D. McGehee, « Accounting for Interference, Scattering, and Electrode Absorption to Make Accurate Internal Quantum Efficiency Measurements in Organic and Other Thin Solar Cells », *Adv. Mater.*, vol. 22, nº 30, p. 3293-3297.
[19] K.-D. Jäger, O. Isabella, A. H. . Smets, R. A. C. M. M. van Swaaij, et M. Zeman, *Solar energy: fundamentals, technology and systems*. 2016.